ISSN 1063-7761, Journal of Experimental and Theoretical Physics, 2008, Vol. 107, No. 1, pp. 140–146. © Pleiades Publishing, Inc., 2008.
Original Russian Text © S.G. Ovchinnikov, 2008, published in Zhurnal Éksperimental'noĭ i Teoreticheskoĭ Fiziki, 2008, Vol. 134, No. 1, pp. 172–178.

Effect of Spin Crossovers on the Mott–Hubbard Transition at High Pressures

S. G. Ovchinnikov

Kirensky Institute of Physics, Siberian Branch, Russian Academy of Sciences, Krasnoyarsk, 660036 Russia
Siberian Federal University, Krasnoyarsk, 660041 Russia
e-mail: sgo@iph.krasn.ru

Received February 1, 2008

Abstract—The effect of spin crossovers in d^n terms on the effective Hubbard parameter (U_{eff}) determining the gap between the lower and upper Hubbard bands is analyzed using a many-electron approach to describe the electron structure of Mott insulators. A new mechanism of the insulator–metal transition is established for d^5 ions, which is related to a decrease in U_{eff} caused by spin crossover. For other ions, the U_{eff} value is either independent of pressure (d^2, d^4, d^7) or it exhibits nonmonotonic growth (d^3, d^6, d^8).

PACS numbers: 71.27.+a, 74.20.-z

DOI: 10.1134/S1063776108070145

1. INTRODUCTION

As is well known, strong electron correlations split the one-electron band in the Hubbard model into the lower and upper Hubbard bands (LHB and UHB, respectively). As the width of this band ($2W$) increases, the gap between the LHB and UHB decreases and, as the bandwidth reaches the critical value $W_c = aU$ (where U is the Hubbard parameter of intraatomic Coulomb repulsion and $a \sim 1$), the Mott–Hubbard transition takes place [1, 2]. An increase in the bandwidth may be related to a decrease in the interatomic distance with increasing pressure or upon isovalent substitution in solid solutions with different ionic radii ("chemical" pressure). The Hubbard parameter U is assumed to be independent of pressure.

For $3d$ metal compounds with predominantly ionic bonding (oxides, halides, etc.), the effects of strong electron correlations determine their dielectric and magnetic properties in the state of Mott insulators. Ideas underlying the Hubbard model have to be supplemented with allowance for the multiorbit character and the presence of anionic sp states. In the low-energy region, the effective Hamiltonian can nevertheless be represented using the generalized Hubbard model, which is constructed on the basis of local d^n, d^{n+1}, and d^{n-1} many-electron terms by analogy with the usual Hubbard model based on the local d^1, d^2, and d^0 terms. An important difference of the generalized Hubbard model from the standard one is that the magnitudes of spins of the d^n, d^{n+1}, and d^{n-1} terms can acquire various values within $0 \leq S \leq 5/2$.

If a cation has an unfilled d shell in the $3d^n$ configuration, an effective Hubbard parameter can be introduced as $U_{\text{eff}} = E_0(d^{n+1}) + E_0(d^{n-1}) - 2E_0(d^n)$ [3]. This quantity determines the gap between the upper Hubbard band with the energy $\Omega_c = E_0(d^{n+1}) - E_0(d^n)$ and the lower Hubbard band with the energy $\Omega_v = E_0(d^n) - E_0(d^{n-1})$, where $E_0(d^n)$ is the energy of the ground term in the d^n configuration. Depending on the relation between Ω_v and the energy ε_v of the top of the occupied band (formed predominantly by the p states of the anion), the dielectric gap E_g is determined either by U_{eff} for $\Omega_v > \varepsilon_v$ (the Mott–Hubbard insulator according to classification [4]) or by $E_g = \Omega_c - \varepsilon_v$ for $\Omega_v < \varepsilon_v$ (the dielectric with charge transfer).

The aim of this study was to elucidate the influence of the interplay of various spin states of d^n ions and the effect of crossovers between these states on the electron structure under conditions of decreasing interatomic distances. It has been established that, in crystals with a local cubic symmetry of cations, U_{eff} depends on the crystal field $\Delta = 10Dq$, which increases with the pressure. At the points of spin crossovers, the dependence $U_{\text{eff}}(\Delta)$ exhibits a change, which is different for various d^n configurations. In particular, U_{eff} decreases upon the crossover for d^5 ions and increases for d^6 ions. In this study, the dependences $U_{\text{eff}}(\Delta)$ were obtained for $1 \leq n \leq 9$. In the systems with d^5 ions (Fe^{3+}, Mn^{2+}), a new mechanism of the Mott–Hubbard transition is revealed, which is determined by a decrease in the electron correlation energy with increasing pressure.

2. SPIN CROSSOVERS IN d^n TERMS

For ionic crystals, the energies of terms for d^n configurations in a cubic crystal field have been determined by numerical methods using the so-called Tanabe–Sugano diagrams [5]. This section reproduces these results within the framework of a simplified model, which provides simple analytical expressions for the energies of terms.This model assumes that (i) all intraatomic Coulomb matrix elements are independent of the orbit number, (ii) the e_g and t_{2g} electrons possess the energies $+6Dq$ and $-4Dq$, respectively, and (iii) each pair of parallel spins provides an energy gain of $-J$ ($J > 0$ is the Hund exchange parameter). Constructing the distribution of n electrons over the t_{2g} and e_g orbitals, one can readily determine the energy of a term with the given spin S.

The d^2 configuration is represented by the term with a spin of $S = 1$ and the energy

$$E_{HS}(d^2) = E_C(d^2) - 8Dq - J, \quad (1)$$

which corresponds to the ground state for all parameters. Here and below, $E_C(d^n)$ is the Coulomb (spin-independent) part of the energy. For the d^3 configuration, the ground state also always has the high spin $S = 3/2$ and the energy

$$E_{HS}(d^3) = E_C(d^3) - 12Dq - 3J. \quad (2)$$

In the case of d^4 ions, there are three possible spin states:

(a) the high-spin (HS) state with $S = 2$ and the energy

$$E_{HS}(d^4) = E_C(d^4) - 6Dq - 6J; \quad (3)$$

(b) the intermediate-spin (IS) state with $S = 1$ and the energy

$$E_{IS}(d^4) = E_C(d^4) - 16Dq - 3J; \quad (4)$$

(c) the low-spin (LS) state with $S = 0$ and the energy

$$E_{LS}(d^2) = E_C(d^2) - 16Dq - 2J. \quad (5)$$

As can be seen, the LS state is always higher by J than the IS state, while the HS and IS states have comparable energies. For $\Delta = 10Dq < 3J$, the HS state is the ground state, whereas for $\Delta > 3J$, the state with $S = 1$ becomes the ground state. In other words, the HS–IS crossover takes place at $\Delta = 3J$.

For d^5 ions, there are two competitive terms:

(a) the HS state with $S = 5/2$ and the energy

$$E_{HS}(d^5) = E_C(d^5) - 10J; \quad (6)$$

(b) the LS state with $S = 1/2$ and the energy

$$E_{LS}(d^5) = E_C(d^5) - 20Dq - 4J, \quad (7)$$

while the intermediate state with $S = 3/2$ is always higher than these two. Here, the HS–LS crossover takes place (like that for d^4 ions) at $\Delta > 3J$.

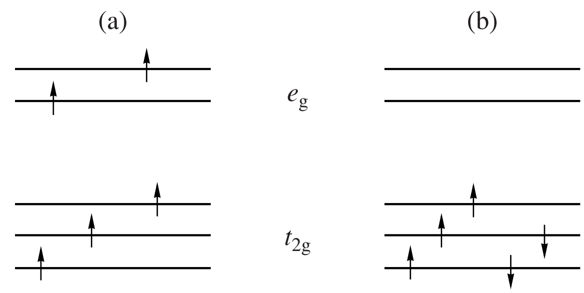

Fig. 1. Schematic diagrams of electron distribution for the d^5 configuration in the (a) high- and (b) low-spin states.

In the case of the d^6 configuration, the IS state is also always higher than the HS and LS terms, which have comparable energies:

(a) the HS state with $S = 2$ and the energy

$$E_{HS}(d^6) = E_C(d^6) - 4Dq - 10J; \quad (8)$$

(b) the LS state with $S = 0$ and the energy

$$E_{LS}(d^6) = E_C(d^6) - 24Dq - 6J, \quad (9)$$

but the HS–LS crossover takes place at a lower value of the crystal field ($\Delta = 2J$) than in the case of d^4 and d^5 ions.

For the d^7 configuration, the possible terms are as follows:

(a) the HS state with $S = 3/2$ and the energy

$$E_{HS}(d^7) = E_C(d^7) - 8Dq - 11J; \quad (10)$$

(b) the LS state with $S = 1/2$ and the energy

$$E_{LS}(d^7) = E_C(d^7) - 18Dq - 9J.$$

In this configuration, the HS–LS crossover takes place (like that for d^6 ions) at $\Delta = 2J$.

The d^8 configuration has only the HS state with $S = 1$ and the energy

$$E_{HS}(d^8) = E_C(d^8) - 12Dq - 13J. \quad (11)$$

Finally, the d^9 configuration has a single state with $S = 1/2$ and the energy

$$E(d^9) = E_C(d^9) - 6Dq - 16J. \quad (12)$$

For example, Fig. 1 shows the distributions of electrons over d orbitals for the HS and LS terms of the d^5 configuration, which illustrate the calculation of energies for these terms.

3. THE MOTT–HUBBARD TRANSITION INDUCED BY THE SPIN CROSSOVER AT HIGH PRESSURES

The effective Hubbard parameter for the d^5 configuration is $U_{eff}(d^5) = E(d^6) + E(d^4) - 2E(d^5)$. An analysis of the terms of d^4, d^5, and d^6 configurations and related

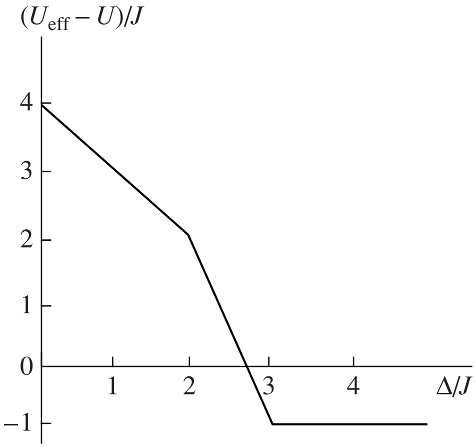

Fig. 2. A plot of the effective Hubbard parameter (U_{eff}) versus crystal field for the d^5 configuration.

crossovers shows that, in U_{eff} calculations, one can distinguish three regions of the Δ/J parameter:

(i) $\Delta/J < 2$. In this case, all terms occur in the HS state and the effective Hubbard parameter is

$$U_{\mathrm{eff}}(d^5) = U(d^5) + 4J - \Delta, \tag{13}$$

where $U(d^5) = E_C(d^6) + E_C(d^4) - 2E_C(d^5)$.

(ii) $2 < \Delta/J < 3$. In this interval, the d^6 configuration passes to the LS state, while the d^5 and d^4 terms remain in the HS state, which yields

$$U_{\mathrm{eff}}(d^5) = U(d^5) + 8J - 3\Delta. \tag{14}$$

(iii) $\Delta/J > 3$. Here, the d^6 and d^5 configurations are in the LS state and the d^4 configuration is in the IS state, so that

$$U_{\mathrm{eff}}(d^5) = U(d^5) - J. \tag{15}$$

Figure 2 presents a plot of the effective Hubbard parameter $U_{\mathrm{eff}}(d^5)$ versus crystal field, which shows that the electron correlations significantly decrease with increasing Δ, the total decrease being $\delta U_{\mathrm{eff}} = 5J - \Delta_0$. For the typical (of $3d$ electrons) values of $J = 0.8$ eV and $\Delta_0 = 1$–2 eV, this yields $\delta U_{\mathrm{eff}} = 2$–$3$ eV. As the pressure increases, the interatomic distance decreases and the crystal field parameter increases. Since the variations of interatomic distances are relatively small, we can assume that, with a good accuracy, this growth can be described by a linear relation as

$$\Delta(P) = \Delta_0 + \alpha_\Delta P, \tag{16}$$

which is apparently violated only at the points of the first-order phase transitions accompanied by a jump in the lattice parameters and the unit cell volume. At such points, the $\Delta(P)$ value for isostructural transitions also changes in a jumplike manner, while the case of transitions involving a change in the crystal symmetry requires calculation of terms in more detail with allowance of the low-symmetry crystal field components. In many cases, such components are small as compared to those for the cubic symmetry and, hence, can be ignored. Apparently, this situation takes place in $FeBO_3$ and $GdFe_3(BO_3)_4$. Spin crossovers and the entire combination of changes in the electron, magnetic, and optical properties of these compounds were studied in our previous publications [6–8]. The jump in U_{eff} observed in these ferroborates was caused by the first-order phase transition involving a volume change at $P \approx 50$ GPa.

The effective Hubbard parameter U_{eff} has a quite simple physical meaning, representing the energy necessary to provide for the d electron hopping between atoms. Indeed, we have two d^n ions in the initial state, while the transfer of an electron from one of these ions to another yields the final state with d^{n+1} and d^{n-1} ions. This very energy gives the criterion for the Mott–Hubbard transition:

$$W_C = aU_{\mathrm{eff}}, \tag{17}$$

where the band halfwidth W also depends on the pressure as

$$W(P) = W_0 + \alpha_W P. \tag{18}$$

It should be noted that the present study is not aimed at the development of a theory of the Mott–Hubbard transition, which was described (within the framework of the Hubbard model) using various methods including split higher Green's functions [9], coherent potential approximation [10], a diagram technique for Hubbard's X-operators [11], and dynamic mean-field theory [12]. We will discuss the realization of criterion (17). As was mentioned in the Introduction, the quantity $U_{\mathrm{eff}} = U_0$ in the standard Hubbard model has a constant value that is independent of pressure. The insulator–metal transition in this model is determined by an increase in the kinetic energy of electrons with increasing pressure. It is the pressure-induced growth in W (so-called bandwidth control) that accounts for the transition.

As was shown above, the situation for d^5 ions (where an increase in the bandwidth is accompanied by a decrease in the correlation energy) significantly differs from that in the Hubbard model. Figure 3 illustrates different variants of the Mott–Hubbard transition for the d^5 configuration by showing the left- and right-hand sides of criterion (17) as functions of pressure. For comparison to the mechanism of band broadening, the dashed line indicates a constant level of $U_0 = U + 4J - \Delta(0)$. Three variants of the linear pressure dependence of the bandwidth $W(P)$ with various coefficients ($\alpha_{W1} > \alpha_{W2} > \alpha_{W3}$) correspond to different scenarios of the transition. In case 1 (strong dependence of the bandwidth on the pressure), the Mott–Hubbard transition proceeds on the background of the HS terms d^5, d^4, and d^6. Here, the points of the intersection of $W_1(P)$ with $U_{\mathrm{eff}}(P)$ and the constant level U_0 (P_{C1} and P^*_{C1}, respectively) differ rather slightly and the main mechanism occurs via band broadening. In case 2 (moderate pressure dependence of the bandwidth $W_2(P)$), the transition takes place in the vicinity of crossovers for all terms (d^5, d^4, and d^6). The true transition corresponds to a significantly lower pressure P_{C2} than that (P^*_{C2}) corresponding to the mechanism of band broadening. Finally, in case 3 (weak dependence of the bandwidth on pressure), it proceeds on the background of LS terms d^5, d^6, and the IS term of the d^4 configuration. Here, $P_{C3} \ll P^*_{C3}$ and the weak dependence on pressure of the bandwidth $W_3(P)$ makes the transition via band broadening impossible, whereas a decrease in the correlation energy $U_{\text{eff}}(P)$ due to the spin crossover significantly decreases the P_{C3} value. Thus, the spin crossover inducing the Mott–Hubbard transition is the dominating mechanism in case 2 and especially in case 3.

In order to quantitatively determine the transition pressure, let us denote by P_{I} and P_{II} the pressures corresponding to the bending points in Fig. 3. These special points obey the relations $\Delta(P_{\text{I}}) = 2J$ and $\Delta(P_{\text{II}} = 3J)$, which yield

$$P_{\text{I}} = \frac{2J - \Delta_0}{\alpha_\Delta}, \quad P_{\text{II}} = \frac{3J - \Delta_0}{\alpha_\Delta}. \tag{19}$$

Assuming for simplicity that the constant coefficient in criterion (17) is $a = 1$, we can write the following conditions for the transition due to the band broadening at P^*_{C} and due to the spin crossover at P_{C} in case 2 (Fig. 3):

$$U_0 = 2(W_0 + \alpha_W P^*_{\text{C}}), \tag{20}$$

$$U + 8J - 3\Delta(P_{\text{C}}) = 2(W_0 + \alpha P_{\text{C}}), \tag{21}$$

where $U_0 = U + 4J - \Delta_0$ is the effective Hubbard parameter at zero pressure. Then, the critical pressures can be expressed as follows:

$$P^*_{\text{C}} = \frac{U_0 - 2W_0}{2\alpha_W}, \tag{22}$$

$$P_{\text{C}} = \frac{U_0 - 2W_0 + 4J - 2\Delta_0}{2\alpha_W + 3\alpha_\Delta}. \tag{23}$$

It is difficult to compare P_{C} and P^*_{C} without knowledge of particular parameters. However, taking into account that $P_{\text{C}} \le P_{\text{II}}$, expression (23) for P_{C} can be approximated as follows:

$$P_{\text{C}} \approx P^*_{\text{C}} - \frac{5J - \Delta_0}{2\alpha_W}. \tag{24}$$

This relation indicates that $P_{\text{C}} < P^*_{\text{C}}$ (since $\Delta_0 < 3J$). The numerical estimates of parameters for $FeBO_3$ and $BiFeO_3$ will be presented below (see Section 6). In particular, the data for $BiFeO_3$ indicate that $P_{\text{C}} \ll P^*_{\text{C}}$.

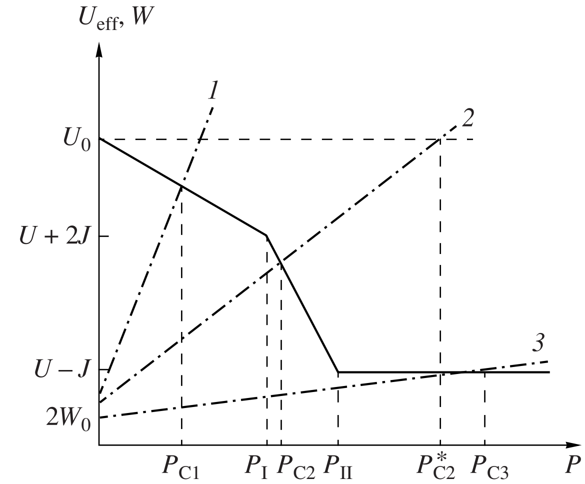

Fig. 3. Schematic diagram illustrating the proposed mechanism of the Mott–Hubbard transition: the solid curve shows $U_{\text{eff}}(P)$; the horizontal dashed line indicates the constant U_0 level; dash–dot lines *1*, *2*, and *3* correspond to different dependences of the Hubbard band width on the pressure as described by Eq. (18) with $\alpha_{W1} > \alpha_{W2} > \alpha_{W3}$, respectively; points P_{C1}, P_{C2}, and P_{C3} correspond to the Mott–Hubbard transition.

4. ELECTRON CORRELATIONS ENHANCED BY THE SPIN CROSSOVER FOR THE d^6 CONFIGURATION

An analysis of the energies of various spin terms for the d^5, d^6, and d^7 configurations as determined from Eqs. (6)–(10) indicate that the effective Hubbard parameter, which can be expressed as

$$U_{\text{eff}}(d^6) = E(d^7) + E(d^5) - 2E(d^6), \tag{25}$$

also behaves differently in the three regions of the Δ/J parameter:

(i) $\Delta/J < 2$. In this case, all terms occur in the HS state and the effective Hubbard parameter is

$$U_{\text{eff}} = U - J.$$

(ii) $2 < \Delta/J < 3$. In this interval, the d^5 term represents the HS state, while the d^6 and d^7 terms correspond to the LS state, which yields

$$U_{\text{eff}} = U + 3\Delta - 7J.$$

(iii) $\Delta/J > 3$. Here, all configurations are in the LS state and

$$U_{\text{eff}} = U - J + \Delta.$$

In contrast to the d^5 configuration, where U_{eff} decreases with increasing crystal field (and pressure), the d^6 configuration exhibits the opposite trend: the correlation energy increases with pressure and the maximum growth is observed in the region of spin crossovers. The possible variants are illustrated in Fig. 4, where the

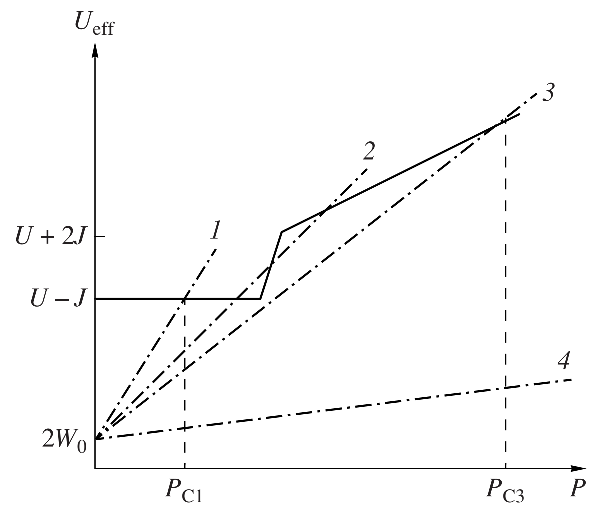

Fig. 4. Plots of U_{eff} versus pressure **P** for the d^6 configuration. Dash–dot lines *1*, *2*, *3*, and *4* correspond to $\alpha_{W1} > \alpha_{W2} > \alpha_{W3} > \alpha_{W4}$, respectively.

dash–dot lines *1–4* correspond to different pressure coefficients α_{W_i}.

In case 1 (strong dependence of the bandwidth W on pressure P), the Mott–Hubbard transition proceeds on the background of the HS terms d^5, d^6, and d^7. Here, the transition mechanism is completely determined by the band broadening. In case 3 (moderate dependence of W on P), the spin crossover significantly increases the gap and the critical pressure (P_{C3}) as compared to those for the mechanism of band broadening. In case 4 ($\alpha_W < \alpha_\Delta$), the transition is impossible and the dielectric phase is retained for all values of parameters. Finally, in rather unusual case 2, the increasing pressure induces the sequence of insulator–metal–insulator–metal transitions; that is, intermediate metallic and dielectric phases appear in the vicinity of spin crossover. This case is possible under the following conditions:

$$\frac{U - J - W_0}{P_{\text{I}}} < \alpha_W < \frac{U + 2J - W_0}{P_{\text{II}}}. \tag{26}$$

5. EFFECTIVE HUBBARD PARAMETERS FOR OTHER CONFIGURATIONS

Using the results of analysis in Section 2, one can readily show that the effective Hubbard parameter for d^2, d^4, and d^7 configurations is independent of the pressure and has a constant value of $U_{\text{eff}} = U - J$. In other words, the spin crossovers that take place for d^4 and d^7 ions do not lead to the dependence of U_{eff} on pressure. In the d^1 and d^9 configurations, the spin crossovers are absent and U_{eff} has the same value ($U - J$). In the multiorbit case, the lower level in the d^2 configuration corresponds to $S = 1$, so that $U_{\text{eff}} = U - J$, where U is the parameter characteristic of the orbitally nondegenerate model with a singlet d^2 term.

For the d^3 and d^8 configurations, the spin crossovers are manifested in the excited states (d^4 and d^7, respectively). Nevertheless, this leads to the following dependence of U_{eff} on the crystal field Δ

(a) For the d^3 configuration:

$$U_{\text{eff}}(\Delta) = \begin{cases} U - J + \Delta, & \Delta < 3J \\ U + 2J, & \Delta > 3J; \end{cases} \tag{27}$$

(b) for the d^8 configuration:

$$U_{\text{eff}}(\Delta) = \begin{cases} U - J + \Delta, & \Delta < 2J \\ U + J, & \Delta > 2J. \end{cases} \tag{28}$$

As can be seen, the correlation energy for these configurations linearly increases with pressure in the region of HS terms d^3, d^4, d^2 as well as d^7, d^8, d^6, and reaches saturation upon a crossover to the LS state. As a result, the critical pressure for the Mott–Hubbard transition is greater than that according to the band broadening mechanism.

6. DISCUSSION OF RESULTS AND COMPARISON TO EXPERIMENT

In recent years, the phenomenon of spin crossover at high pressure in 3d metal oxides has been extensively studied. This interest is primarily related to basic problems of the physics of the condensed state, in particular, to the formation of a dielectric state due to strong electron correlations and the Mott–Hubbard transition. In addition, the properties of iron oxides at high pressures are of interest in geophysics, since these compounds enter into the composition of many minerals constituting the Earth's mantle [13]. Spin crossovers have been found and studied in various crystals, including $FeBO_3$ [14], $GdFe_3(BO_3)_4$ [7], and $BiFeO_3$ [15], where all cases involve Fe^{3+} ions in the d^5 configuration. An analysis of experimental data using the many-electron approach described above requires knowledge of both the parameters at $P = 0$ (including the Coulomb interaction parameter U, the exchange interaction parameter J, the bandwidth $2W$, and the crystal field Δ) and the pressure coefficients α_W and α_Δ. For ferroborates, these parameters have been determined from a comparison to the experimental data [6, 7] and calculated from first principles [16].

For $FeBO_3$, the dielectric gap decreases from 3 eV in the HS state to 0.8 eV in the LS state. This behavior agrees well with the decrease in U_{eff} as depicted in Fig. 3. In $FeBO_3$ and $GdFe_3(BO_3)_4$, the band halfwidth W is small and its pressure dependence is weak because of low p–d hybridization typical of oxyborides. This is related to the fact that the sp hybridization inside the BO_3 group is very pronounced and the p orbitals of oxygen are deformed so strongly that their hybridization with the cation is negligibly small. This conclusion is confirmed by ab initio calculations [17]. The pressure dependence of the bandwidth $W(P)$ in ferroborates corresponds to case 3 (Fig. 3), where the transition pressure P_{C3} is greater than the maximum values (140 GPa) for which the conductivity was experimentally studied [18].

The model parameters for $FeBO_3$ are as follows [8]:

$$U_0 = 4.2 \text{ eV}, \quad J = 0.8 \text{ eV}, \quad \Delta_0 = 1.5 \text{ eV},$$
$$W_0 = 0.36 \text{ eV}, \quad \alpha_W = 0.002 \text{ eV/GPa}, \qquad (29)$$
$$\alpha_\Delta = 0.02 \text{ eV/GPa}.$$

Accordingly, the transition pressure for $FeBO_3$ (in case 3, Fig. 3) is as follows:

$$P_C = (U_0 - 2W - 5J + \Delta_0)/2\alpha_W = 250 \text{ GPa}. \qquad (30)$$

An analogous spin crossover between HS and LS states of Fe^{3+} in $BiFeO_3$ takes place in the same pressure range (about 50 GPa) as in ferroborates. However, in contrast to ferroborates, the crossover in $BiFeO_3$ is accompanied by the insulator–metal transition [15]. The main distinction of the electron structure of $BiFeO_3$ from that of ferroborates is related to a stronger *p–d* hybridization, that is, a greater bandwidth $W(P)$. This situation is described by case 2 in Fig. 3, where the spin crossover leads to a sharp decrease in U_{eff}. This decrease induces the Mott–Hubbard transition at a pressure (P_{C2}) that is much lower than that (P^*_{C2}) corresponding to the usual mechanism of band broadening. This case apparently corresponds to $BiFeO_3$. Unfortunately, the model parameters for this compound are not available. However, we can suggest that enhancement of the covalent effects will primarily influence the bandwidth and take the following estimates:

$$W_0 = 0.6 \text{ eV}, \quad \alpha_W = 0.006 \text{ eV/GPa}.$$

Other parameters not directly related to the covalent properties will be taken the same as for $FeBO_3$ (see (29)). Then, using formula (22) and the data given in (23), we obtain

$$P^*_C = 250 \text{ GPa}, \quad P_C = 44.4 \text{ GPa}.$$

It should be noted that the calculation of P_C using simplified formula (24) yields $P_C = 41.7$ GPa, which demonstrates the validity of this formula for $P_{II} - P_C \ll P_C$. The experimental value for $BiFeO_3$ is $P_C \approx 54$ GPa, which confirms the adequacy of parameters used for $BiFeO_3$.

The covalence not only increases the width of the *d* band, but it can also contribute to the competition of various spin states. Indeed, it was recently demonstrated by means of the exact diagonalization of the multielectron Hamiltonian of the MeO_6 cluster for Me = Fe^{2+}, Co^{3+} (i.e., for the d^6 cation) [19] that, for certain parameters of the system, the IS state with $S = 1$ can be stabilized. However, this conclusion is only valid for a rather specific set of parameters and cannot be treated as the general case. In the general case, the main effects of the *p–d* hybridization are an increase in the *d–d* hopping integral, the width of the *d* band, and superexchange parameter.

In conclusion, it has been established that the effective Hubbard parameter exhibits a dependence on pressure, which is most pronounced in the vicinity of spin crossovers. For d^5 ions, the correlation effects are significantly suppressed, whereas for d^6 ions these effects are enhanced with increasing pressure. In other configurations, the pressure dependence is either weak or absent.

ACKNOWLEDGMENTS

The author is grateful to D. Homsky, G. Sawatzky, and M. Haverkort for fruitful discussions of results.

This study was supported by the Russdian Foundation for Basic Research (project no. 07-02-00226) and the Presidium of the Russian Academy of Sciences (Program “Quantum Macrophysics”). This study was initiated during the author’s work at the Kavli Institute for Theoretical Physics (University of California, Santa Barbara, USA) and supported by the NSF (grant no. PHY05-51164).

REFERENCES

1. N. F. Mott, *Metal–Insulator Transitions* (Taylor and Francis, London, 1974).
2. J. C. Hubbard, Proc. R. Soc. London, Ser. A **276**, 238 (1963).
3. J. Zaanen and G. A. Sawatzky, J. Solid State Chem. **88**, 8 (1990).
4. J. Zaanen, G. A. Sawatzky, and J. W. Allen, Phys. Rev. Lett. **55**, 418 (1985).
5. Y. Tanabe and S. Sugano, J. Phys. Soc. Jpn. **9**, 753 (1954).
6. A. G. Gavriliuk, I. A. Trojan, S. G. Ovchinnikov, et al., Zh. Éksp. Teor. Fiz. **126** (3), 650 (2004) [JETP **99** (3), 566 (2004)].
7. A. G. Gavriliuk, S. A. Kharlamova, I. S. Lyubutin, et al., Pis’ma Zh. Éksp. Teor. Fiz. **80** (6), 482 (2004) [JETP Lett. **80** (6), 426 (2004)].
8. S. G. Ovchinnikov, J. Magn. Magn. Mater. **300**, 243 (2006).
9. J. C. Hubbard, Proc. R. Soc. London, Ser. A **281**, 401 (1964).
10. B. Velicky, S. Kirkpatrick, and H. Ehrenreich, Phys. Rev. **175**, 747 (1968).
11. R. O. Zaitsev, Zh. Éksp. Teor. Fiz. **70** (3), 1100 (1976) [Sov. Phys. JETP **43** (3), 574 (1976)].

12. A. Georges, G. Kotliar, W. Krauth, and M. Rozenberg, Rev. Mod. Phys. **68**, 13 (1996).
13. S. A. Gramsch, R. E. Cohen, and S. Yu. Savrasov, Am. Mineral. **88**, 257 (2003).
14. V. A. Sarkisyan, I. A. Troyan, I. S. Lyubutin, et al., Pis'ma Zh. Éksp. Teor. Fiz. **76** (11), 788 (2002) [JETP Lett. **76** (11), 664 (2002)].
15. A. G. Gavriliuk, V. V. Struzhkin, I. S. Lyubutin, et al., Phys. Rev. B **77**, 155112 (2008).
16. S. G. Ovchinnikov, V. I. Anisimov, I. A. Nekrasov, and Z. V. Pchelkina, Phys. Met. Metallogr. **99** (Suppl. 1), 93 (2005).
17. A. V. Postnikov, St. Bartkowski, M. Neumann, et al., Phys. Rev. B: Condens. Matter **50**, 14849 (1994).
18. I. A. Troyan, M. I. Eremets, A. G. Gavrilyuk, et al., Pis'ma Zh. Éksp. Teor. Fiz. **78** (1), 16 (2003) [JETP Lett. **78** (1), 13 (2003)].
19. S. G. Ovchinnikov and Yu. S. Orlov, Zh. Éksp. Teor. Fiz. **131** (3), 485 (2007) [JETP **104** (3), 436 (2007)].

Translated by P. Pozdeev